ACS PHYSICAL CHEMISTRY Au
AN OPEN ACCESS JOURNAL OF THE AMERICAN CHEMICAL SOCIETY

pubs.acs.org/physchemau
Perspective

Theoretical Insights into the Dynamics of Gas-Phase Bimolecular Reactions with Submerged Barriers

Hongwei Song* and Hua Guo*

Cite This: ACS Phys. Chem Au 2023, 3, 406–418
Read Online
ACCESS | Metrics & More | Article Recommendations

ABSTRACT: Much attention has been paid to the dynamics of both activated gas-phase bimolecular reactions, which feature monotonically increasing integral cross sections and Arrhenius kinetics, and their barrierless capture counterparts, which manifest monotonically decreasing integral cross sections and negative temperature dependence of the rate coefficients. In this Perspective, we focus on the dynamics of gas-phase bimolecular reactions with submerged barriers, which often involve radicals or ions and are prevalent in combustion, atmospheric chemistry, astrochemistry, and plasma chemistry. The temperature dependence of the rate coefficients for such reactions is often non-Arrhenius and complex, and the corresponding dynamics may also be quite different from those with significant barriers or those completely dominated by capture. Recent experimental and theoretical studies of such reactions, particularly at relatively low temperatures or collision energies, have revealed interesting dynamical behaviors, which are discussed here. The new knowledge enriches our understanding of the dynamics of these unusual reactions.

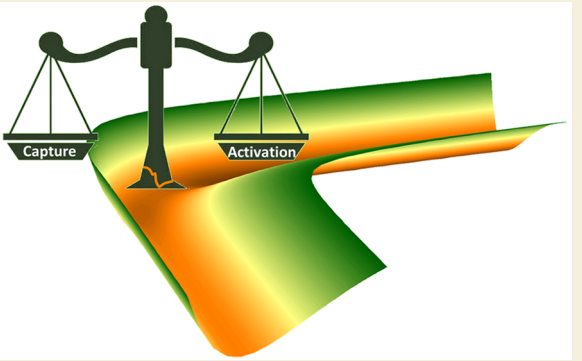

KEYWORDS: *submerged barrier, bimolecular reaction, mode specificity, product energy disposal, rate coefficient, quantum effect, non-Arrhenius behavior*

1. INTRODUCTION

Most bimolecular chemical reactions involve an activation barrier due to the simple fact that an old bond is broken as a new bond is formed. In the gas phase, these reactions are typically characterized by Arrhenius kinetics, in which the rate coefficient increases exponentially with temperature.[1] This so-called Arrhenius behavior suggests the existence of a barrier along the reaction path (see Figure 1); overcoming this barrier requires a certain amount of energy. As a result, such reactions are more facile at high temperatures. The activation energy can be derived from the slope of the Arrhenius plot, where the log of the rate coefficient is a linear function of the inverse temperature. Investigations of the dynamics of such reactions in the gas phase have revealed that the activation can be enabled by the relative kinetic energy of the collision partners.[2−7] Indeed, the corresponding reaction cross section typically increases with collision energy, which improves the chances of crossing the reaction barrier.[8] In addition, the activation can also be facilitated by excitation in internal degrees of freedom of reactants, such as vibration and in some cases rotation, provided the energy can help to overcome the barrier. This has been demonstrated by preparing specific excited reactant internal states using, for example, lasers.[9] Importantly, the efficacy of different reactant modes in promoting reactivity may differ, leading to mode specificity,[10−13] which, along with the related

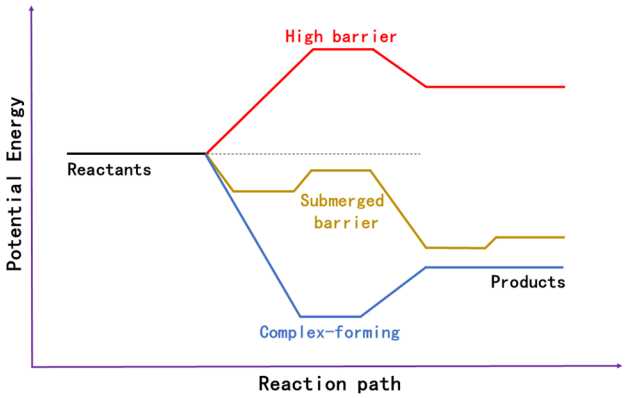

Figure 1. Schematic diagram of the reaction paths of different types of bimolecular reactions.

Received: March 8, 2023
Revised: June 2, 2023
Accepted: June 6, 2023
Published: June 27, 2023

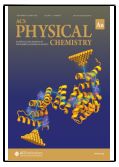

https://doi.org/10.1021/acsphyschemau.3c00009
ACS Phys. Chem Au 2023, 3, 406–418

bond selectivity, is a result of dynamics. The relative efficacy of a reactant mode can be rationalized by Polanyi's rules,[14] which state that a reaction with an "early" barrier is best promoted by collision energy, while a reaction with a "late" barrier is helped more effectively by reactant vibrational excitation. Here, the "early" or "late" barrier refers to the similarity of the transition state with either the reactant or the product configuration. Recently, we proposed the sudden vector projection (SVP) model[15,16] to better understand and predict mode specificity, and it has been shown to be quite successful for many activated gas-phase reactions.[17,18] Within the SVP model, the efficacy of a reactant mode in promoting the reaction is attributed to its coupling with the reaction coordinate at the transition state, quantified by the overlap between the two corresponding normal mode vectors. The SVP model is amenable to reactions involving polyatomic reactants which have multiple vibrational modes. It is also applicable to rotational modes.

There also exists another class of bimolecular reactions that need no activation. The rate coefficient of such a reaction typically decreases with temperature (negative temperature dependence), defying the Arrhenius norm.[19,20] Obviously, such reactions are of great importance in low-temperature environments such as interstellar media, but they may also play important roles in many other situations, including planetary atmospheres, plasmas, and combustion. The nonactivated nature stems from the fact that the reaction path is barrierless, as schematically shown in Figure 1, which is common for ion−molecule reactions and reactions involving free radicals. Many kinetic and dynamical studies of such reactions have been carried out in recent years.[21−27] Most such reactions are dominated by long-range interactions, which allow the two reactants to be captured by a deep potential well supporting a reaction intermediate.[19,28] As a result, the corresponding reaction cross section often has no threshold and decreases with increasing collision energy, due to the long-range capture with large impact parameters.[8] In fact, the kinetics can be reliably described by simple capture theories,[28−31] such as that of Langevin.[32] If the intermediate is long lived, significant energy randomization may occur among all of the internal degrees of freedom in the reactive system, which could erase all memory of the reactants. Hence, dynamical features such as mode specificity are typically absent, and the reaction is often amenable to a statistical treatment.[33−36]

In this Perspective, we discuss an interesting case between the two extremes mentioned above. In such a reaction, there exists no intrinsic barrier on the potential energy surface (PES) along the reaction coordinate, but the reaction is controlled by a submerged saddle point (SP) along the reaction path, which provides a bottleneck. As illustrated in Figure 1, the submerged SP is flanked by pre- and post-SP wells, which could be due to chemical bonding,[37] hydrogen bonding,[38,39] or weak covalent interactions such as three-electron two-center hemibonds.[40,41] Hence, such a reaction might share some characteristics of a barrierless capture reaction such as negative temperature-dependent rate coefficients but might also have some features in common with an activated reaction such as mode specificity. These behaviors underscore the competition between different microscopic reaction mechanisms which might coexist for these reactions. It is worth noting that these characteristics might also be present for reactions with very low barriers. Importantly, such reactions are commonly seen in low-temperature astronomic and atmospheric environments and have received increasing attention in recent years.[29,42,43] In this Perspective, we focus on several prototypical reactions of this type and review recent theoretical advances in understanding the corresponding dynamics using quantum mechanical and/or classical methods. We will strive to present the discussion in the context of available experimental data. We will also restrict our discussion to adiabatic systems in which the rearrangement of chemical bonds occurs on a single Born−Oppenheimer PES. The reader is referred to recent reviews on nonadiabatic dynamics for bimolecular reactions in the literature.[44,45]

2. THEORETICAL METHODS

2.1. Potential Energy Surfaces

Theoretical studies of chemical dynamics rely on accurate global PESs, which can be constructed from high-level electronic structure calculations. For small reactive systems with relatively light atoms, it is now possible to construct chemically accurate (errors < 1 kcal mol^{-1}) PESs. This is typically done with the calculation of the electronic energy at different nuclear geometries using a high-level ab initio method, such as the coupled cluster (CC) or multireference configuration interaction (MRCI) method.[46] However, it should be noted that, in most cases, chemical accuracy is still difficult to achieve. The energies at discrete points are then represented by an analytic function of the nuclear coordinates using, for example, a machine learning method such as one based on neural networks.[47] Much progress has been made in recent years, and excellent reviews have been published for the construction of global PESs for reactive systems.[48−56] For this reason, we will not provide a thorough discussion here.

2.2. Quantum Reactive Scattering

Since molecular systems are intrinsically quantum mechanical, the ultimate characterization of the reaction dynamics can only be achieved using a quantum scattering method. A major challenge in reactive quantum scattering is the exponential increase of computational costs with respect to the size of the problem.[57] There are two approaches to quantum dynamics (QD), solving either the time-independent (TID) or the time-dependent (TD) Schrödinger equation.[57] The TID method requires matrix inversion and thus scales cubically with the dimensionality. On the other hand, the TD approach is more efficient as it solves an initial value problem by propagating a wave packet, which has better scaling laws with respect to the size of the problem. The TD approach can also be formulated using the Chebyshev propagation method, in which the effective time is given by the Chebyshev order.[58,59] In this Perspective, we will thus discuss only the wave packet approaches.

The wave packet approaches for computing initial state-selected total reactivity[60,61] are intuitive and relatively straightforward. Here, we take a penta-atomic reactive system X + YABC to briefly introduce the method considering that most of the discussed reactions in this Perspective involve five atoms. The full-dimensional Hamiltonian in the reactant Jacobi coordinates with a given total angular momentum J_{tot} can be written as ($\hbar$ = 1 hereafter)[62,63]

$$\hat{H} = -\frac{1}{2\mu_R}\frac{\partial^2}{\partial R^2} - \frac{1}{2\mu_1}\frac{\partial^2}{\partial r_1^2} - \frac{1}{2\mu_2}\frac{\partial^2}{\partial r_2^2} - \frac{1}{2\mu_3}\frac{\partial^2}{\partial r_3^2} + \frac{(\hat{J}_{tot} - \hat{j})^2}{2\mu_R R^2} + \frac{\hat{l}_1^2}{2\mu_1 r_1^2} + \frac{\hat{l}_2^2}{2\mu_2 r_2^2} + \frac{\hat{j}_3^2}{2\mu_3 r_3^2} + \hat{V}(R, r_1, r_2, r_3, \theta_1, \theta_2, \theta_3, \varphi_1, \varphi_2) \quad (1)$$

where $\boldsymbol{R}$ is the Jacobi vector from the center of mass (COM) of the YABC molecule to the atom X, $\boldsymbol{r}_1$ is the vector from the COM of ABC to the atom Y, $\boldsymbol{r}_2$ is the vector from the COM of BC to the atom A, and $\boldsymbol{r}_3$ is the vector from atom C to atom B, with μ_R, μ_1, μ_2, and μ_3 as their corresponding reduced masses. $\hat{j}_3$ is the rotational angular momentum operator of the moiety BC, and $\hat{l}_2$ is the orbital angular momentum operator along $\boldsymbol{r}_2$. The coupling of $\hat{l}_3$ and $\hat{l}_2$ gives rise to $\hat{j}_{23}$. $\hat{l}_1$ is the orbital angular momentum operator along $\boldsymbol{r}_1$, and its coupling with $\hat{j}_{23}$ generates $\hat{J}$. $\hat{J}_{tot}$ is the total angular momentum operator of the system.

https://doi.org/10.1021/acsphyschemau.3c00009
ACS Phys. Chem Au 2023, 3, 406−418

This Hamiltonian has been successfully used in treating the dynamics of the H + NH_3 reaction,[62,64,65] and more recently the F + NH_3 reaction.[66]

The parity (ε) adapted wave function is expanded in terms of the body-fixed (BF) ro-vibrational basis functions

$$\psi^{J_{tot}M\varepsilon}(\mathbf{R}, \mathbf{r}_1, \mathbf{r}_2, \mathbf{r}_3) = \sum_{n,\nu,j,K} C_{n\nu jK}^{J_{tot}M\varepsilon} u_n^{\nu_1}(R)\phi_{\nu_1}(r_1)\phi_{\nu_2}(r_2)\phi_{\nu_3}(r_3) \Phi_{jK}^{J_{tot}M\varepsilon}(\hat{R}, \hat{r}_1, \hat{r}_2, \hat{r}_3) \quad (2)$$

where $C_{n\nu jK}^{J_{tot}M\varepsilon}$ are expansion coefficients, $u_n^{\nu_1}(R)$ are sine translational basis functions, ν denotes the vibrational basis indices (ν_1,ν_2,ν_3), and $\phi_{\nu_i}(r_i)$ is obtained by solving the one-dimensional (1D) reference Hamiltonians defined as

$$\hat{h}_i(r_i) = -\frac{1}{2\mu_i}\frac{\partial^2}{\partial r_i^2} + V_i^{ref}(r_i),\ i = 1, 3 \quad (3)$$

where $V_i^{ref}(r_i)$ are the corresponding 1D reference potentials and j represents (l_1,l_2,j_3,j_{23},J). $\Phi_{jK}^{J_{tot}M\varepsilon}$ in eq 2 is the parity-adapted coupled BF total angular momentum eigenfunction, which can be written as[62]

$$\Phi_{jK}^{J_{tot}M\varepsilon} = (1 + \delta_{K0})^{-1/2}\sqrt{\frac{2J_{tot}+1}{8\pi}}[\bar{D}_{K,M}^{J_{tot}} Y_{l_{j_{23}}l_{j_3}}^{JK} + \varepsilon(-1)^{l_1+l_2+j_3+J+J_{tot}}\bar{D}_{-K,M}^{J_{tot}} Y_{l_{j_{23}}l_{j_3}}^{J-K}] \quad (4)$$

where $D_{K,M}^J$ is the Wigner rotation matrix,[67] M is the projection of J_{tot} on the space-fixed (SF) z axis, K is the projection of J_{tot} on the BF z axis, which is defined to coincide with the vector $\boldsymbol{R}$, and $Y_{l_{j_{23}}l_{j_3}}^{JK}$ is the eigenfunction of the angular momentum operator $\hat{J}$, which is defined as

$$Y_{l_{j_{23}}l_{j_3}}^{JK} = \sum_{\omega}\bar{D}_{K\omega}^{J}(\hat{r}_1)\sqrt{\frac{2l_1+1}{2J+1}}\langle j_{23}\omega l_1 0|J\omega\rangle Y_{j_{23}l_{j_3}\omega}(\hat{r}_2, \hat{r}_3) \quad (5)$$

and

$$Y_{j_{23}l_{j_3}\omega}(\hat{r}_2, \hat{r}_3) = \sum_{m}\bar{D}_{\omega m}^{j_{23}}(\hat{r}_2)\sqrt{\frac{2l_2+1}{2j_{23}+1}}\langle j_3 m l_2 0|j_{23}m\rangle y_{j_3 m}(\hat{r}_3) \quad (6)$$

where y_{jm} denotes spherical harmonics and ω is the projection of the angular momentum J on the vector $\boldsymbol{r}_1$. Note the restriction that $\varepsilon(-1)^{l_1+l_2+j_3+J+J_{tot}} = 0$ for $K = 0$ in eq 4.

The initial wave packet $|\chi_i\rangle$ is built as a direct product of a Gaussian wave packet along the scattering coordinate R and a specific ro-vibrational state of the reactant YABC in the BF representation

$$|\chi_i\rangle = \left(\frac{1}{\pi\delta^2}\right)^{1/4} e^{-(R-R_0)^2/2\delta^2} e^{-ik_0R}|v_0 j_0 \tau; J_{tot}K\varepsilon\rangle \quad (7)$$

where R_0 and δ are the mean position and width of the initial Gaussian function and $k_0 = \sqrt{2\mu_R E_i}$ is the mean momentum. v_0, j_0, and τ denote the initial vibrational state, total angular momentum, and parity of the reactant YABC, respectively.

Two evolution operators are often employed to propagate the wave packet: the second-order split-operator method[68] and the real Chebyshev propagator.[69−71] In the former, the time evolution operator is approximated in the short time limit by the second-order split-operator propagator implemented as follows

$$|\psi(t+\Delta)\rangle = \exp(-i\Delta\hat{T}/2)\exp(-i\Delta\hat{V})\exp(-i\Delta\hat{T}/2)|\psi(t)\rangle \quad (8)$$

in which Δ is the time step and the approximation arises from the noncommutativity of $\hat{T}$ and $\hat{V}$.

The Chebyshev propagator is a cosine evolution operator in the Chebyshev order domain, which can be transformed to the energy domain via a discrete cosine Fourier transform.[70,72] In the Chebyshev order domain, the wave packet is propagated as follows

$$|\psi_{k+1}\rangle = D(2\hat{H}_{scaled}|\psi_k\rangle - D|\psi_{k-1}\rangle),\ k \geq 1 \quad (9)$$

where $|\psi_1\rangle = D\hat{H}_{scaled}|\psi_0\rangle$, $|\psi_0\rangle = |\chi_i\rangle$, and D is a damping function (vide infra). The scaled Hamiltonian is defined as $\hat{H}_{scaled} = (\hat{H} - H^+)/H^-$ to avoid the divergence of the Chebyshev polynomials outside the range $[-1, 1]$.[73] Here, the spectral medium and half-width of the Hamiltonian $H^{\pm} = (H_{max} \pm H_{min})/2$ are calculated from the spectral extrema H_{min} and H_{max}. The discrete Chebyshev propagator is exact and typically more efficient,[74] since the time propagator requires some forms of approximation.

The total reaction probability from a specific initial state is calculated by

$$P_{v_0 j_0 \tau K_0}^{J_{tot}\varepsilon}(E_c) = \langle\chi_i^+(E)|\hat{F}|\chi_i^+(E)\rangle \quad (10)$$

in which E_c is the collision energy. The flux through the dividing surface $S(r_1 = r_1^F)$ is calculated from the energy-dependent scattering wave function $|\chi_i^+(E)\rangle$ that is obtained by Fourier transforming the wave packet on a dividing surface.[75]

The total reaction integral cross section (ICS) from a specific initial state is computed by summing the reaction probabilities over all relevant partial waves

$$\sigma_{v_0 j_0 \tau}(E_c) = \frac{1}{(2j_0+1)}\sum_{K_0\varepsilon}\frac{\pi}{k^2}\sum_{J_{tot}\geq K_0}(2J_{tot}+1)P_{v_0 j_0 \tau K_0}^{J_{tot}\varepsilon}(E_c) \quad (11)$$

where $k = \sqrt{2\mu E_c}$ and μ is the reduced mass between the reactants. The differential cross section (DCS) can, in principle, be computed from the S-matrix elements,[57] but the calculation of the latter involves complex coordinate transforms and is rarely attempted beyond tetratomic systems.[5,6,76]

The initial state-specific rate coefficient is calculated by thermal averaging the collision energy of the corresponding ICS as

$$k_{v_0 j_0 \tau}(T) = \sqrt{\frac{8k_BT}{\pi\mu}}\frac{1}{(k_BT)^2}\int_0^{\infty} dE_c E_c \exp(-E_c/k_BT)\sigma_{v_0 j_0 \tau}(E_c) \quad (12)$$

where k_B is the Boltzmann constant. The thermal rate coefficient is then obtained by Boltzmann averaging of the initial state-specific rate coefficients as

$$k(T) = \frac{\sum_{v_0 j_0}(2j_0+1)k_{v_0 j_0 \tau}(T)\exp(-E_{v_0 j_0}/k_BT)}{\sum_{v_0 j_0}(2j_0+1)\exp(-E_{v_0 j_0}/k_BT)} \quad (13)$$

2.3. Quasi-Classical Trajectory

While a quantum mechanical treatment of the reactive scattering is preferred, the numerical cost of such calculations quickly becomes unaffordable as the size increases.[57] As an inexpensive alternative, quasi-classical trajectory (QCT) methods have been widely applied to study reactions.[77,78] In the QCT approach, the atomic coordinates and momenta of reactants are prepared in specific quantum states using ad hoc quantization conditions, and the subsequent classical dynamics on the PES is followed by solving the Hamilton's equations. Such a QCT method has been implemented in software such as VENUS 96.[79] Unlike quantum dynamics, the reactivity is simulated using a statistical approach in which a swarm of trajectories with a random sampling of initial conditions is propagated and the final state distributions are averaged over the reactive trajectories. Although QCT cannot describe quantum effects, such as tunneling and resonances, a large number of studies have demonstrated its reasonable accuracy for a wide range of reactions, particularly for highly averaged quantities such as rate coefficient and total cross section.[23,80−84]

In the QCT approach, the ICS of the reaction is calculated by

$$\sigma_r(E_c) = \pi b_{max}^2\frac{N_r}{N_{tot}} \quad (14)$$

where N_r and N_{tot} are the numbers of reactive and total trajectories at a collision energy E_c. The impact parameter (b) is sampled from a uniformly distributed random number $\zeta \in [0,1]$ according to b =

https://doi.org/10.1021/acsphyschemau.3c00009
ACS Phys. Chem Au 2023, 3, 406−418

$b_{max}\zeta^{1/2}$, where the maximum impact parameter b_{max} is determined by small batches of trajectories with trial values at each specified initial condition. The relative statistical error is given by $\Delta = \sqrt{(N_{tot} - N_r)/N_{tot}N_r}$.

The DCS is computed by

$$\frac{d\sigma_r}{d\Omega} = \frac{\sigma_r P_r(\theta)}{2\pi \sin(\theta)} \quad (15)$$

where $P_r(\theta)$ is the normalized reaction probability and Ω is the scattering solid angle. The scattering angle θ is defined as

$$\theta = \cos^{-1}\left(\frac{\vec{v}_i \cdot \vec{v}_f}{|\vec{v}_i||\vec{v}_f|}\right) \quad (16)$$

in which $\vec{v}_i$ and $\vec{v}_f$ denote the initial and final relative velocities. $P_r(\theta')$ is calculated by

$$P_r(\theta') = \frac{\sum_{\theta \geq \theta' - \Delta\theta'}^{\theta < \theta' + \Delta\theta'} N_r(\theta)}{N_r} \quad (17)$$

The rate coefficient at temperature T is then obtained by

$$k(T) = \left(\frac{8k_B T}{\pi\mu}\right)^{1/2} \pi b_{max}^2 \frac{N_r}{N_{tot}} \quad (18)$$

Here, the initial rovibrational energies of the reactants and the collision energy are sampled according to the Boltzmann and Maxwell–Boltzmann distributions, respectively, while the sampling of the impact parameter is the same as that discussed above.

One issue associated with all trajectory-based dynamical methods is the treatment of the quantization of product internal modes. Since classical mechanics does not observe energy quantization, binning of trajectories is needed. The simplest way is to use the histogram binning (HB) method, in which the classical action variable is binned to the closest integer.[77] However, the HB approach does not discriminate different action variables in the same binning box, and this can sometimes be problematic for zero-point energy (ZPE)-violating trajectories. A more reasonable approach is the Gaussian binning (GB),[85−87] in which a Gaussian weight is assigned to each trajectory depending on the difference between the calculated action variable and the nearest quantum number. There is ample evidence indicating that GB is more accurate than HB.[87] For polyatomic molecules, the original GB scheme becomes very computationally demanding, and simplified approaches have been proposed.[88−90]

3. PROTOTYPICAL REACTIONS

For a chemical reaction with a submerged barrier, as mentioned above, there exist pre- and post-SP wells along the reaction path. In this work, we focus on reactions with relatively shallow pre- and post-SP wells, since if the pre- and/or post-SP well(s) are too deep, the reaction tends to behave statistically. Table 1 lists the barrier heights and depths of pre- and post-SP wells of some prototypical reactions, most of which have been investigated by both experiment and theory. We will discuss below important dynamical (and kinetic to a lesser extent) features of these reactions using these examples.

3.1. Differential and Integral Cross Sections

Barrierless capture reactions typically manifest forward−backward DCSs and monotonically decaying ICSs as a function of the collision energy, while activated reactions often feature forward or backward domination of the DCS and monotonically increasing excitation function. For reactions with a submerged barrier, there is sometimes competition between these two coexisting mechanisms.

An example that attracted much recent attention is the highly exoergic hydrogen abstraction of ammonia by a fluorine atom, F + NH_3 → HF + NH_2. This reaction has a barrierless reaction path with a submerged barrier flanked by a pre-SP and a much deeper post-SP well,[39,91] as shown in Figure 2. Since the submerged barrier is merely 11.774 kcal mol^{-1} below the reactant asymptote and slightly higher than the pre-SP well, the reaction can proceed directly or undergo trapping in the pre- and/or post-SP wells. The trapping leads to indirect mechanisms.

Table 1. Energies (in kcal mol^{-1}) of the Submerged Barrier, Pre- and Post-SP Wells, and Products of a Selected Group of Reactions with Submerged Barriers[a]

reactions	pre-SP well	SP	post-SP well	products
$NH_2^- + H_2 \rightarrow H^- + NH_3$	−4.24[b]	−1.39[b]	−14.57[b]	−5.79[b]
$OH^+ + H_2 \rightarrow H + H_2O^+$	−10.92[c]	−5.58[c]	−29.61[c]	−23.70[c]
$H_2O^+ + H_2 \rightarrow H_3O^+ + H$	−7.36[d]	−4.64[d]	−43.60[d]	−40.63[d]
$NH_2^+ + H_2 \rightarrow NH_3^+ + H$	−3.10[e]	−2.83[e]	−30.78[e]	−28.85[e]
$HO + CO \rightarrow CO_2 + H$	−2.26[f]	−0.58[f]	−29.59[f]	−22.62[f]
$F + NH_3 \rightarrow HF + NH_2$	−13.73[g]	−11.77[g]	−36.16[g]	−26.19[g]
$OH + HO_2 \rightarrow H_2O + O_2$	−3.25[h]	−1.60[h]	-	−70.57[h]
$OH + H_2S \rightarrow H_2O + SH$	−3.36[i]	−0.10[i]	−32.67[i]	−29.68[i]
$F + CH_3OH \rightarrow HF + CH_3O$	−6.70[j]	−5.04[j]	−36.56[j]	−28.52[j]

[a]The energies are given with respect to the reactant asymptote. [b]Reference 104, at the level of UCCSD(T)/aug-cc-pVTZ′, with Z′ denoting an additional diffuse basis set for the N atom. [c]Reference 114, at the level of MRCI+Q/aug-cc-pVQZ. [d]Reference 110, at the level of UCCSD(T)-F12b/aug-cc-pVTZ. [e]Reference 126, at the level of UCCSD(T)-F12a/aug-cc-pVTZ. [f]Reference 101, at the level of UCCSD(T)-F12b/aug-cc-pVTZ. [g]Reference 39, at the level of UCCSD(T)-F12/aug-cc-pVTZ. [h]The lowest triplet state, ref 95, at the level of CCSD(T)-F12a/aug-cc-pVTZ. [i]Reference 122, at the level of UCCSD(T)-F12a/aug-cc-pVTZ. [j]Reference 106, at the level of UCCSD(T)-F12a/aug-cc-pVTZ.

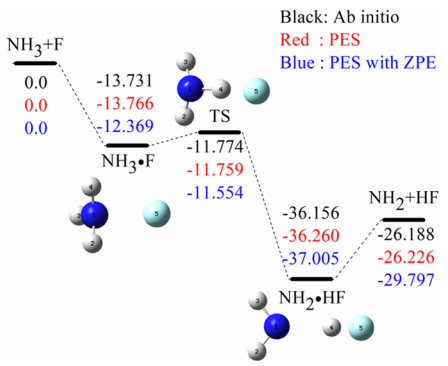

Figure 2. Schematic diagram of the reaction path for the F + NH_3 → HF + NH_2 reaction. The ab initio energies of the stationary points at the level of UCCSD(T)-F12/aug-cc-pVTZ (black), the values of the fitted PES (red), and the zero-point energy-corrected values (blue) are shown below the corresponding geometries. All energies are given in kcal mol^{-1} and relative to the reactant asymptote. Reproduced with permission from ref 39. Copyright 2019 Royal Society of Chemistry.

Experimentally, the measured DCSs at relatively low collision energies show a strong forward bias, with non-negligible sideways and backward components.[92] The dominant forward scattering can be attributed to a direct stripping mechanism, in which the incoming F picks up an H with large impact parameters, while the backward scattering is due apparently to direct rebound with small impact parameters. As shown in

https://doi.org/10.1021/acsphyschemau.3c00009
ACS Phys. Chem Au 2023, 3, 406−418

Figure 3, these behaviors were reproduced by QCT calculations on full-dimensional PESs.[39,91] On the other hand, most indirect

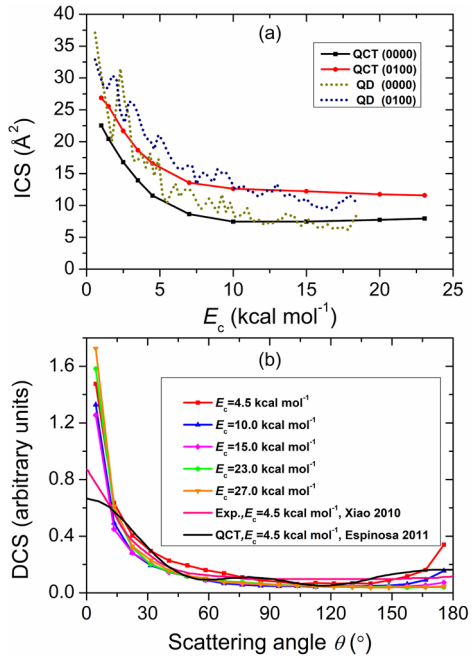

Figure 3. (a) QD and QCT ICSs of the F + NH_3 → HF + NH_2 reaction from the ground and fundamental states of NH_3 as a function of the collision energy. The four quantum numbers (ν_1, ν_2, ν_3, ν_4) in parentheses denote excitation in the symmetric stretching, umbrella, asymmetric stretching, and asymmetric bending modes of NH_3, respectively. (b) The corresponding DCSs from the ground state with the collision energy E_c fixed at 4.5, 10.0, 15.0, 23.0, and 27.0 kcal mol^{-1} together with Xiao et al.'s experimental results[92] and Espinosa-García et al.'s theoretical results.[91] Adapted with permission from refs 39 and 66. Copyrights 2019 and 2021 Royal Society of Chemistry.

trajectories originate from large impact parameter collisions, for which the shallow pre-SP well plays a more significant role than the post-SP well in trapping the colliders. These indirect trajectories produce a near-isotropic angular distribution, superimposed on the DCS from the direct channel, consistent with the experimental observation.[92] These indirect trajectories suggest possible existence of metastable quantum resonances, which have been identified in a more recent joint experiment–theory study of the $[FNH_3]^-$ photodetachment.[93]

The excitation function for this reaction, namely, the dependence of the reactive ICS with collision energy, has not been measured experimentally, but the QCT results shown in Figure 3 suggest an initial fast decay of the ICS as a function of the collision energy, followed by a slight rise above 15 kcal mol^{-1}.[39] This is consistent with the coexistence of direct and indirect mechanisms, as discussed above, on the anisotropy of the DCS. Indeed, as the collision energy increases, the forward scattering is enhanced, indicating the decreased importance of the indirect channel, in agreement with the rise of the ICS. The excitation function was studied by the quantum wave packet method as well.[66] The QD ICS has a similar overall collision energy dependence to the QCT result, which initially decreases sharply and then levels off with the increase of collision energy. Nevertheless, there exist significant oscillations in the QD ICS, implying again the possible existence of quantum resonances. In addition, both QD and QCT ICSs suggest an enhancement of reactivity with the excitation of the bending (0100) mode of NH_3.

More recently, a combined experimental and theoretical study of photodetachment of the $[FNH_3]^-$ anion, which probes the dynamics of the neutral reaction near its transition state, has provided strong evidence of Feshbach resonances in both wells near the transition state.[93] Calculated resonance wave functions showed that most resonances are associated with the significant HF vibrational excitation, coupled with excitation of soft modes such as the HF–NH_2 translational mode, pseudorotation of HF, and the torsional modes of NH_2. Interestingly, some high-energy resonances were found across the transition state and extended into the pre-SP well, which may impact the bimolecular reaction dynamics. These results are consistent with the oscillatory ICS observed in the previous QD study,[66] although a more thorough investigation of the bimolecular reaction dynamics is needed to elucidate the role of the resonances.

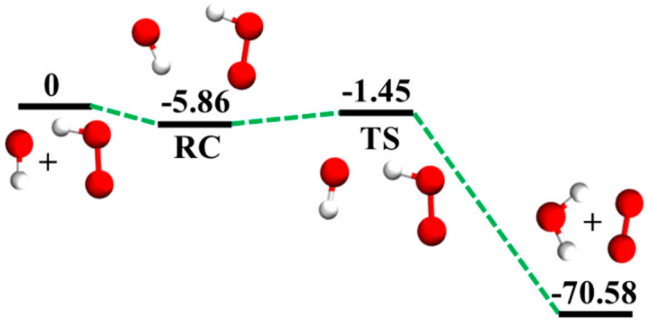

Figure 4. Schematic energetics for the OH + HO_2 → H_2O + O_2 reaction on the lowest triplet state PES. Energies are in kcal mol^{-1} and relative to the OH + HO_2 asymptote. Reproduced with permission from ref 96. Copyright 2020 American Chemical Society.

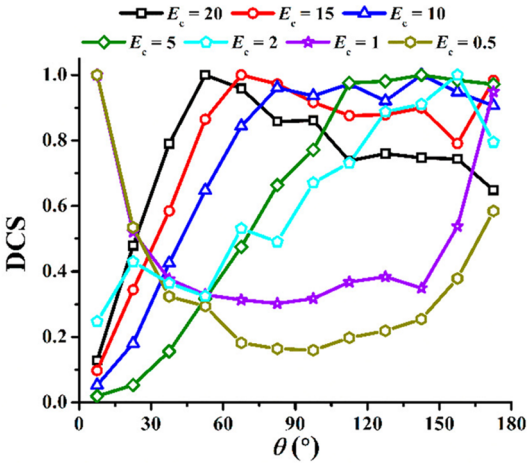

Figure 5. QCT DCSs at different E_c (in kcal mol^{-1}) for ground-state reactants for the OH + HO_2 → H_2O + O_2 reaction. Reproduced with permission from ref 96. Copyright 2020 American Chemical Society.

Another recent example is the OH + HO_2 → H_2O + O_2 reaction, which has important implications in atmospheric chemistry.[94] Similar to the F + NH_3 case, this reaction features a slightly submerged barrier, as shown in Figure 4.[95] QCT studies on a full-dimensional ab initio based PES[95] showed (Figure 5) a dramatic transition from an indirect complex-forming mechanism at low collision energies, evidenced by near-symmetric backward–forward DCSs, to forward-dominated DCSs at

https://doi.org/10.1021/acsphyschemau.3c00009
ACS Phys. Chem Au 2023, 3, 406–418

higher collision energies, resulting apparently from an increasing importance of the direct stripping mechanism.[96] Similar to the F + NH_3 reaction discussed above, the excitation function displays an initial decay followed by a slight rise at higher collision energies.

It is interesting to note that the existence of a submerged barrier does not always lead to meaningful competition between the two mechanisms. In the OH + CO → CO_2 + H reaction, which plays a key role in combustion and the atmosphere,[97] the dominant reaction channel is controlled by two bottlenecks, TS1 and TS2, as shown in Figure 6. The QCT reaction

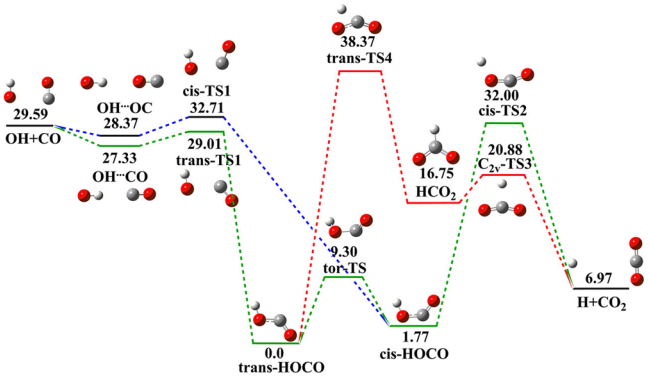

Figure 6. Energetics of the reaction pathways for the HO + CO → H + CO_2 reaction. The ab initio energies of the stationary points are given in kcal mol^{-1} relative to the *trans*-HOCO minimum. Reproduced with permission from ref 154. Copyright 2012 American Chemical Society.

probability first increases monotonically and then becomes more or less flat with the increasing collision energy. In contrast, the QD probability shows many narrow resonances apparently due to the long-lived HOCO.[98,99] The QCT ICS shown in Figure 7 is a monotonically increasing function of the collision energy. The measured DCS (Figure 7) shows a near-isotropic distribution with a slight forward bias,[100] which is satisfactorily reproduced by QCT calculations. This can be understood in terms of the energy of the submerged SP, which is barely below the reactant asymptote.[101,102]

Similar behaviors of DCSs and ICSs have also been found in many reactions with submerged barriers, such as NH_2^- + H_2 → H^- + NH_3,[103,104] OH^+ + H_2 → H + H_2O^+,[105] and F + CH_3OH → HF + CH_3O.[106]

3.2. Rate Coefficients

A characteristic feature of a barrierless capture reaction is a negative temperature dependence of its thermal rate coefficient. This non-Arrhenius behavior can be attributed to the lack of an activation barrier and the long-range attractive interaction, which favor capture at very low collision energies.[107] Such kinetics is related to the monotonically decaying excitation function.[8] For reactions with a submerged barrier, the temperature dependence of the rate coefficients can be more complex, containing both negative and positive temperature dependences in different temperature regions. This phenomenon is prevalent in chemical kinetics,[29,30] as highlighted by a recent combined experimental and theoretical study of oxygen-atom reactions with alkenes at low temperatures.[108]

The ion−molecule H_2O^+ + H_2 → H_3O^+ + H reaction, which is believed to be involved in the interstellar water formation,[109] has no intrinsic barrier, but its reaction pathway features a submerged SP, as shown in Figure 8.[110] Experimentally, the

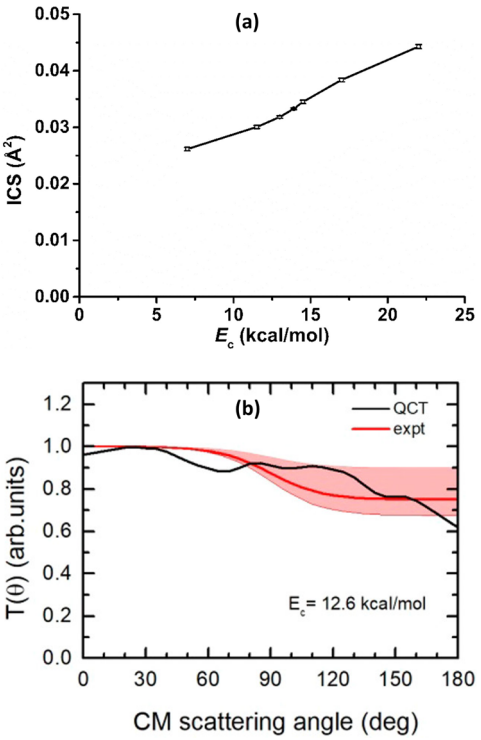

Figure 7. (a) QCT ICSs for the OH + CO → H + CO_2 reaction as a function of the collision energy. (b) Best-fit CO_2 angular distribution and comparison with QCT results at E_c = 12.6 kcal mol^{-1}. Adapted with permission from ref 100. Copyright 2018 American Chemical Society.

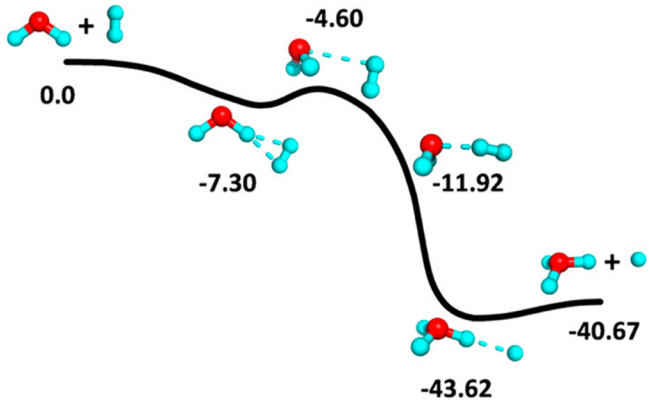

Figure 8. Schematic depiction of the PES along the reaction coordinate for the H_2O^+ + H_2 → H_3O^+ + H reaction. The geometries and energies (in kcal mol^{-1}) of the stationary points are provided. Reproduced with permission from ref 111. Copyright 2014 American Chemical Society.

measured rate coefficient exhibits weak and complex temperature dependence between 100 and 600 K with a maximum at ∼350 K, as shown in Figure 9.[111] The experiment was reproduced by QCT calculations[111] on an ab initio-based PES.[110] This complex temperature dependence cannot be explained by the excitation function, which decays monotonically with the collision energy.[112,113] Instead, it was rationalized by the competition between an enhancement of reactivity (vide infra) by low-lying rotationally excited states of H_2O^+ and a general decrease in efficiency at higher collision energies for this barrierless reaction. Specifically, the slightly positive temperature dependence at low temperatures results apparently from rotational enhancement of the rate coefficient. On the other

https://doi.org/10.1021/acsphyschemau.3c00009
ACS Phys. Chem Au 2023, 3, 406−418

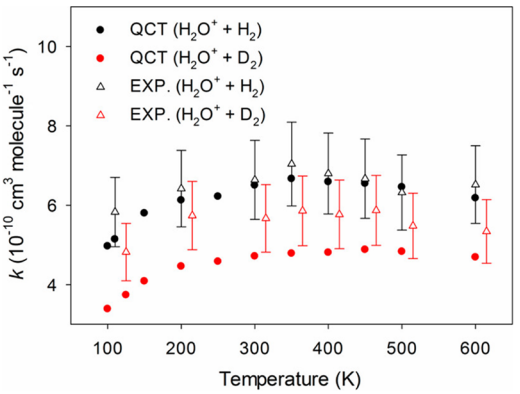

Figure 9. Comparison of the measured and computed rate coefficients for the $H_2O^+ + H_2$ and $H_2O^+ + D_2$ reactions, with 15% relative error bars shown. The experimental data for D_2 have been offset for clarity. Reproduced with permission from ref 111. Copyright 2014 American Chemical Society.

hand, the decrease of the rate coefficient at higher temperatures is attributable to the submerged barrier, which rises with the increasing orbital angular momentum. It was found that the dissociation of the pre-SP complex back to reactants through the loose entrance channel increases faster than its decomposition to products over the tighter transition state as the collision energy increases, resulting in a decreasing rate coefficient.[111] Similarly, the thermal rate coefficient of the $OH^+ + H_2 \rightarrow H_2O^+ + H$ reaction calculated on an ab initio PES[114] also exhibits weak temperature dependence from 200 to 600 K.[115]

Complex and non-Arrhenius rate coefficients have been observed in several other reactions with submerged barriers, including the $F + NH_3 \rightarrow HF + NH_2$,[39,116] $F + CH_3OH \rightarrow HF + CH_3O$,[117] $Cl + CH_3OH \rightarrow HCl + CH_2OH$,[118] and $OH + HO_2 \rightarrow H_2O + O_2$ reactions.[95]

3.3. Mode Specificity

Since a barrierless capture reaction does not have an intrinsic barrier, it typically possesses no strong dependence on the type of energy imparted into the reactants,[24] in sharp contrast to an activated reaction. However, the lack of mode specificity does not always hold when the reaction has a submerged barrier, because the effective barrier could emerge above the reactant asymptote at large impact parameters due to the centrifugal potential. This effective barrier provides a reaction bottleneck which might induce mode specificity.

An interesting example is the $H_2O^+ + H_2 \rightarrow H_3O^+ + H$ reaction, which was found experimentally to have strong rotational mode specificity. Specifically, the ICS of the reaction is enhanced by H_2O^+ rotational excitation.[119,120] Apparently, this rotational enhancement effect is also responsible for the observed temperature dependence of the rate coefficient, as discussed above.[111] As shown in Figure 8, this reaction has a submerged barrier, which could serve as a bottleneck for the reaction. To understand the surprising mode specificity, QD and QCT calculations have been performed on an ab initio PES, and they reproduced the experimental observations satisfactorily, as shown in Figure 10.[112,121] The mode specificity can be understood with the SVP model,[17] which attributes the ability of a reactant mode to enhance the reaction to its coupling with the reaction coordinate at the relevant transition state. In the sudden limit, such coupling can be quantified by the projection of the reactant mode onto the reaction coordinate. In this case, the submerged barrier can be considered as the transition state.

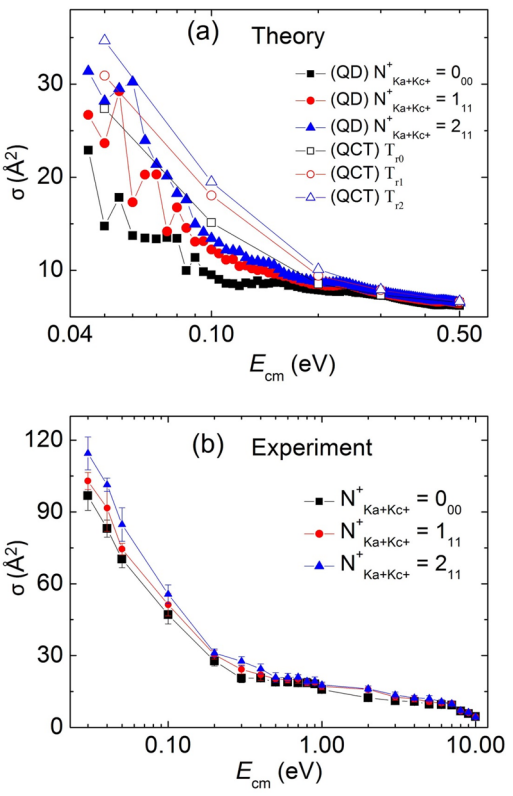

Figure 10. (a) Theoretical QD and QCT ICSs $\sigma(H_3O^+$: 000; 0_{00}, 1_{11}, and $2_{11})$ values in Å^2 calculated at E_c = 0.04−0.50 eV. For QCT calculations, the 0_{00}, 1_{11}, and 2_{11} energies are specified by the rotational temperatures, T_{r0}, T_{r1}, and T_{r2}, respectively. (b) Experimental $\sigma(H_3O^+$: 000; 0_{00}, 1_{11}, and $2_{11})$ values in Å^2 obtained at E_c = 0.03−10.00 eV. Reproduced with permission from ref 112. Copyright 2016 Royal Society of Chemistry.

The SVP model revealed that the rotational modes of H_2O^+ are strongly coupled with the reaction coordinate, thus leading to the promotional effect.[112] We note in passing that such rotational mode specificity cannot be easily explained by the Polanyi rules.

Vibrational mode specificity was also experimentally observed for this reaction.[112,119,120] In contrast to the promotional effect of the rotational modes, the excitation of H_2O^+ vibrational modes inhibits the reactivity. QCT calculations successfully reproduced the experimental observations,[112] but a simple explanation of the large inhibitory effects remains elusive. (Note that the SVP model cannot predict inhibitory effects.) This example underscores the potential role played by a submerged barrier for mode-specific reaction dynamics.

Mode specificity has also been examined for the $F + NH_3 \rightarrow HF + NH_2$ reaction using both QD and QCT methods.[66] These calculations showed that excitation of every NH_3 vibrational mode promotes the reaction. Surprisingly, the low-frequency umbrella mode has the largest efficacy compared to the other three normal modes. The significant promotional effect of the umbrella mode was explained by the enlarged attractive interaction between F and NH_3 that increases the chance of capturing F by NH_3 in the pre-SP well and the modulation of the submerged barrier that enhances the direct reaction. This is confirmed by the SVP model, showing that the umbrella mode has the largest projection on the reaction coordinate at the submerged transition state, followed by the asymmetric and symmetric stretching modes.

https://doi.org/10.1021/acsphyschemau.3c00009
ACS Phys. Chem Au 2023, 3, 406−418

A surprising mode specificity was recently reported for OH + HO_2 → H_2O + O_2.[96] QCT calculations showed that the excitation of the H−OO stretch has a significant promotional effect, due apparently to the motion of the breaking OH bond in HO_2. Excitations in the H−O−O bend and O−O stretch present smaller enhancement effects on the reactivity at low collision energy. Surprisingly, vibrational excitation of the OH reactant, which is considered a spectator for the reaction, shows a significant enhancement effect at collision energies below 5.0 kcal mol^{-1}. The unusual enhancement effect, which is not predicted by the SVP model, was ascribed to the increased dipole of the vibrationally excited OH, which increases its attractive interaction with HO_2 and thus effectively deepens the pre-SP well. The deepening of the pre-SP well favors the capture of the colliders at low collision energies, therefore enhancing the reactivity. This mode specificity thus differs from the ones discussed above.

We note that mode specificity has also been found in other reactions with submerged barriers, including the neutral OH + H_2S → H_2O + SH[122,123] and OH + CO → H + CO_2 reactions[124,125] and ion−molecule OH^+ + H_2 → H + H_2O^+,[105] H_2 + NH_2^- → H^- + NH_3,[103,104] and H_2 + NH_2^+ → H + NH_3^+ reactions.[126]

3.4. Product Energy Disposal

Many barrierless reactions involve the formation of a reaction intermediate, typically supported by one or more deep wells. Since the lifetime of the intermediate can be quite long, vibrational energy randomization often takes place. A complete energy randomization leads to statistical distributions of the scattering angle and product internal states, which can thus be described by statistical theories.[24,127,128] However, many such reactions do not always lead to statistical product distributions for various reasons, even when there are no submerged barriers.[129−132] For reactions with submerged barriers, as discussed below, this may also be true. This is mostly due to the insufficient lifetime of the intermediate for complete energy randomization.

The product energy disposal of the F + NH_3/ND_3 reactions was investigated by a QCT method.[39] It was found that the available energy largely flows into the vibrational mode of HF, followed by the translational mode and the vibrational modes of NH_2. On the other hand, energy cannot effectively channel into the rotational modes of HF and NH_2. These theoretical results were consistent with earlier experimental observations.[133,134] Furthermore, the HF product is largely populated in the fundamental and first overtone states, followed by the ground and second overtone states. In contrast, the product NH_2 is mainly populated in the ground state, followed by the fundamental state of the bending mode. The propensity can be explained by the SVP model, which stipulates that the energy flow is largely determined by the projection of the product mode onto the reaction coordinate at the transition state.[17] Since the reaction is dominated by a direct stripping mechanism and most of indirect trajectories are trapped in the shallow pre-SP well, the intermediate complex in the post-SP well is apparently not sufficiently long lived to lead to complete energy randomization.

We want to emphasize that the nonstatistical product distribution is not unique to reactions with submerged barriers. Rather, it is a reflection of the extent of energy randomization in the reaction intermediate in all complex-forming reactions.

4. CONCLUSIONS AND PROSPECTS

A direct activated reaction typically manifests unique characteristics, including Arrhenius kinetics, a monotonically increasing ICS, a strongly anisotropic DCS, mode specificity, and possibly nonstatistical product internal state distributions. These features are clearly the result of an activation barrier, which controls both the reaction dynamics and the kinetics. On the other hand, a barrierless capture reaction often behaves completely differently, with negative temperature dependence of the reaction rate, a monotonically decaying ICS, a forward−backward symmetric DCS, and/or statistical product distributions. These characteristics result from the barrierless reaction path with one or more potential wells that are capable of supporting long-lived reaction intermediate(s).

Different from both the activated and the barrierless capture archetypes, reactions with a submerged barrier might exhibit seemingly contradicting behaviors, such as a forward−backward symmetric DCS coexisting with a decaying excitation function. The discussion in this Perspective demonstrates the rich dynamical and kinetic signatures of submerged barrier reactions, dictated by the unique reaction path with a submerged saddle point flanked by pre- and post-SP minima. This submerged barrier could serve as the activation barrier in certain conditions, leading to features belonging to an activated reaction. Such behaviors typically dominate at high collision energies. The barrierless entrance channel and the potential minima, on the other hand, may endow the reaction with traits of a capture process, especially at low collision energies. The quantitative topography of the PES, particularly the relative energy of the stationary points, apparently controls the presence of the competition between direct and indirect mechanisms, which are manifested in differential and integral cross sections, mode specificity, product energy disposal, and temperature dependence of thermal rate coefficients. Several prototypes are discussed in this Perspective to illustrate these unique features.

We mention in passing that the choice of reactions discussed in this Perspective is by no means exhaustive, but we strive to provide a panoramic view of the recent advances with a small number of prototypes. An obvious omission is gas-phase S_N2-type reactions, which bear many similarities to those discussed in this Perspective. The reason that such ion−molecule reactions are not included here is that excellent reviews are already available in the literature.[25,27,135]

We also emphasize that the close collaboration between theory and experiment offers significant synergy in gaining deep insights into the dynamics and kinetics of such reactions. Theoretically, recent advances in quantum chemistry and fitting PESs with machine learning methods have revolutionized our ability to tackle difficult problems that were impossible to imagine a few decades ago. However, there is still a long way to go before we achieve complete understanding of the relevant physics. Since reactions with submerged barriers often are not statistical, their chemical dynamics needs be explicitly characterized. Quantum mechanical treatments are still challenging because of the exponential scaling; classical methods are often sufficient to provide mechanistic insights. New theoretical advances on quantum dynamics are highly desired to provide accurate and efficient characterization of reaction dynamics in full dimensionality.

It is important to note that the reactions discussed in this Perspective are all assumed to be adiabatic, involving a single PES. In reality, many such reactions might involve more than

https://doi.org/10.1021/acsphyschemau.3c00009
ACS Phys. Chem Au 2023, 3, 406−418

one electronic state, and transitions between different electronic states might impact the reactivity, sometimes in a significant way. Examples of such nonadiabatic bimolecular reactions include the reactive quenching of electronically excited OH(A) by H_2,[136] which is facilitated by derivative coupling, and the $F(^2P) + CH_4$ reaction,[137] which is facilitated by spin−orbit coupling. Because nonadiabatic transitions are a quantum effect, the dynamics should be treated quantum mechanically, as reported in several recent studies.[138,139] However, a full quantum treatment is very challenging, so approximate methods for handling nonadiabatic transitions are highly advantageous.[140] Such nonadiabatic reaction dynamics is of current research interest, but discussion of nonadiabatic reactions with a submerged barrier has so far remained scarce. Taking the $F + NH_3$ reaction as an example, the $F(^2P)$ reactant has three spin−orbit sublevels, which are correlated to three electronic states that are coupled via spin−orbit coupling. Future work on such systems will be needed to assess the impact of the breakdown of the Born−Oppenheimer approximation.

Another exciting new frontier is cold and ultracold chemistry,[107,141−147] in which the reactions necessarily require the absence of an intrinsic reaction barrier.[148,149] So far, many cold collision studies have focused on nonreactive scattering,[142,147] but progress has already been made for cold reactive scattering.[107,146] For instance, the reactivity of the slightly exoergic $KRb + KRb \rightarrow K_2 + Rb_2$ reaction has recently been elucidated at the state-to-state level near 200 nK.[150,151] This reaction proceeds without a barrier via an extremely long-lived intermediate in which energy randomization is likely to be close to completion.[152] While most of the measured state-to-state reaction probabilities[151] are in reasonably good agreement with statistical theory predictions,[153] there are some outliers that are not fully understood. New experimental techniques for preparing chemically relevant reactive species at cold and ultracold temperatures will inevitably lead to future challenges to theory, and the role played by a submerged barrier in low-temperature reactivity can be explored in a pure quantum regime.

AUTHOR INFORMATION

Corresponding Authors

Hongwei Song − *State Key Laboratory of Magnetic Resonance and Atomic and Molecular Physics, Innovation Academy for Precision Measurement Science and Technology, Chinese Academy of Sciences, Wuhan 430071, China;* orcid.org/0000-0001-8401-2364; Email: hwsong@wipm.ac.cn

Hua Guo − *Department of Chemistry and Chemical Biology, University of New Mexico, Albuquerque, New Mexico 87131, United States;* orcid.org/0000-0001-9901-053X; Email: hguo@unm.edu

Complete contact information is available at: https://pubs.acs.org/10.1021/acsphyschemau.3c00009

Author Contributions

H.S. and H.G.: conceptualization (lead), funding acquisition (lead), resources (lead), supervision (lead), data curation (lead), writing—original draft (lead), writing—review and editing (lead). CRediT: **Hongwei Song** conceptualization (equal), funding acquisition (equal), investigation (equal), methodology (equal), project administration (equal), resources (equal), supervision (equal), writing-original draft (equal), writing-review & editing (equal); **Hua Guo** conceptualization (equal), funding acquisition (equal), investigation (equal), methodology (equal), project administration (equal), resources (equal), supervision (equal), writing-original draft (equal), writing-review & editing (equal).

Notes

The authors declare no competing financial interest.

ACKNOWLEDGMENTS

This work was supported by the National Natural Science Foundation of China under Grant No. 21973109 to H.S., the Department of Energy under Grant No. DE-SC0015997 to H.G., and the Air Force Office of Scientific Research under Grant No. FA9550-22-1-0350 to H.G. We thank Shaun Ard, Cheuk Ng, Anyang Li, Jun Li, Xixi Hu, Nick Schuman, Al Viggiano, Minghui Yang, and Daiqian Xie for collaboration and for many stimulating discussions.

REFERENCES

(1) Steinfeld, J. I.; Francisco, J. S.; Hase, W. L. *Chemical Kinetics and Dynamics*; Prentice Hall, 1989.
(2) Casavecchia, P. Chemical reaction dynamics with molecular beams. *Rep. Prog. Phys.* **2000**, *63*, 355−414.
(3) Althorpe, S. C.; Clary, D. C. Quantum scattering calculations on chemical reactions. *Annu. Rev. Phys. Chem.* **2003**, *54*, 493−529.
(4) Yang, X. State-to-state dynamics of elementary bimolecular reactions. *Annu. Rev. Phys. Chem.* **2007**, *58*, 433−459.
(5) Zhang, D. H.; Guo, H. Recent advances in quantum dynamics of bimolecular reactions. *Annu. Rev. Phys. Chem.* **2016**, *67*, 135−158.
(6) Fu, B.; Shan, X.; Zhang, D. H.; Clary, D. C. Recent advances in quantum scattering calculations on polyatomic bimolecular reactions. *Chem. Soc. Rev.* **2017**, *46*, 7625−7649.
(7) Pan, H.; Liu, K.; Caracciolo, A.; Casavecchia, P. Crossed beam polyatomic reaction dynamics: recent advances and new insights. *Chem. Soc. Rev.* **2017**, *46*, 7517−7547.
(8) Liu, K. Excitation functions of elementary chemical reactions: a direct link from crossed-beam dynamics to thermal kinetics ? *Int. Rev. Phys. Chem.* **2001**, *20*, 189−217.
(9) Zare, R. N. Laser control of chemical reactions. *Science* **1998**, *279*, 1875−1879.
(10) Crim, F. F. Bond-selected chemistry: vibrational state control of photodissociation and bimolecular reaction. *J. Phys. Chem.* **1996**, *100*, 12725−12734.
(11) Crim, F. F. Vibrational state control of bimolecular reactions: Discovering and directing the chemistry. *Acc. Chem. Res.* **1999**, *32*, 877−884.
(12) Crim, F. F. Chemical dynamics of vibrationally excited molecules: Controlling reactions in gases and on surfaces. *Proc. Natl. Acad. Sci. U.S.A.* **2008**, *105*, 12654−12661.
(13) Liu, K. Vibrational control of bimolecular reactcions with methane with mode-, bond-, and stereo-selectivity. *Annu. Rev. Phys. Chem.* **2016**, *67*, 91−111.
(14) Polanyi, J. C. Some concepts in reaction dynamics. *Science* **1987**, *236*, 680−690.
(15) Jiang, B.; Guo, H. Relative efficacy of vibrational vs. translational excitation in promoting atom-diatom reactivity: Rigorous examination of Polanyi's rules and proposition of sudden vector projection (SVP) model. *J. Chem. Phys.* **2013**, *138*, 234104.
(16) Jiang, B.; Guo, H. Control of mode/bond selectivity and product energy disposal by the transition state: The $X + H_2O$ (X = H, F, $O(^3P)$, and Cl) reactions. *J. Am. Chem. Soc.* **2013**, *135*, 15251−15256.
(17) Guo, H.; Jiang, B. The sudden vector projection model for reactivity: Mode specificity and bond selectivity made simple. *Acc. Chem. Res.* **2014**, *47*, 3679−3685.
(18) Guo, H.; Liu, K. Control of chemical reactivity by transition state and beyond. *Chem. Sci.* **2016**, *7*, 3992−4003.

(19) Troe, J. The colourful world of complex-forming bimolecular reactions. *J. Chem. Soc. Faraday Trans.* **1994**, *90*, 2303−2317.
(20) Klippenstein, S. J.; Pande, V. S.; Truhlar, D. G. Chemical kinetics and mechanisms of complex systems: A perspective on recent theoretical advances. *J. Am. Chem. Soc.* **2014**, *136*, 528−546.
(21) Casavecchia, P.; Balucani, N.; Alagia, M.; Cartechini, L.; Volpi, G. G. Reactive scattering of oxygen and nitrogen atoms. *Acc. Chem. Res.* **1999**, *32*, 503−511.
(22) Balucani, N.; Capozza, G.; Leonori, F.; Segoloni, E.; Casavecchia, P. Crossed molecular beam reactive scattering: from simple triatomic to multichannel polyatomic reactions. *Int. Rev. Phys. Chem.* **2006**, *25*, 109−163.
(23) Aoiz, F. J.; Bañares, L.; Herrero, V. J. Dynamics of insertion reactions of H_2 molecules with excited atoms. *J. Phys. Chem. A* **2006**, *110*, 12546−12565.
(24) Guo, H. Quantum dynamics of complex-forming bimolecular reactions. *Int. Rev. Phys. Chem.* **2012**, *31*, 1−68.
(25) Xie, J.; Otto, R.; Mikosch, J.; Zhang, J.; Wester, R.; Hase, W. L. Identification of atomic-level mechanisms for gas-phase $X^{--} + CH_3Y$ S_N2 reactions by combined experiments and simulations. *Acc. Chem. Res.* **2014**, *47*, 2960−2969.
(26) Osborn, D. L. Reaction mechanisms on multiwell potential energy surfaces in combustion (and atmospheric) chemistry. *Annu. Rev. Phys. Chem.* **2017**, *68*, 233−260.
(27) Meyer, J.; Wester, R. Ion−molecule reaction dynamics. *Annu. Rev. Phys. Chem.* **2017**, *68*, 333−353.
(28) Clary, D. C. Fast chemical reactions: Theory challenges experiment. *Annu. Rev. Phys. Chem.* **1990**, *41*, 61−90.
(29) Smith, I. W. M. Reactions at very low temperatures: Gas kinetics at a new frontier. *Angew. Chem., Int. Ed.* **2006**, *45*, 2842−2861.
(30) Klippenstein, S. J.; Georgievskii, Y. Theory of Low Temperature Gas-Phase Reactions. In *Low Temperatures and Cold Molecules*; Smith, I. W. M., Ed.; Imperial College Press: London, 2008; pp 175−229.
(31) Tsikritea, A.; Diprose, J. A.; Softley, T. P.; Heazlewood, B. R. Capture theory models: An overview of their development, experimental verification, and applications to ion−molecule reactions. *J. Chem. Phys.* **2022**, *157*, 060901.
(32) Langevin, M. P. Une formule fondamentale de théorie cinétique. *Ann. Chim. Phys.* **1905**, *5*, 245−288.
(33) Pechukas, P.; Light, J. C.; Rankin, C. Statistical theory of chemical kinetics: Application to neutral-atom-molecule reactions. *J. Chem. Phys.* **1966**, *44*, 794.
(34) Miller, W. H. Study of the statistical model for molecular collisions. *J. Chem. Phys.* **1970**, *52*, 543−551.
(35) Quack, M.; Troe, J. Specific Rate Constants of Unimolecular Processes II. Adiabatic Channel Model. *Ber. Bunsenges. Phys. Chem.* **1974**, *78*, 240−252.
(36) Rackham, E. J.; Gonzalez-Lezana, T.; Manolopoulos, D. E. A rigorous test of the statistical model for atom-diatom insertion reactions. *J. Chem. Phys.* **2003**, *119*, 12895−12907.
(37) Kudla, K.; Schatz, G. C.; Wagner, A. F. A quasiclassical trajectory study of the OH+CO reaction. *J. Chem. Phys.* **1991**, *95*, 1635−1647.
(38) Li, J.; Dawes, R.; Guo, H. An ab initio based full-dimensional global potential energy surface for $FH_2O(X^2A')$ and dynamics for the $F + H_2O \rightarrow HF + HO$ reaction. *J. Chem. Phys.* **2012**, *137*, 094304.
(39) Tian, L.; Zhu, Y.; Song, H.; Yang, M. Theoretical study of the $F(^2P) + NH_3 \rightarrow HF + NH_2$ reaction on an accurate potential energy surface: dynamics and kinetics. *Phys. Chem. Chem. Phys.* **2019**, *21*, 11385−11394.
(40) Monge-Palacios, M.; Espinosa-Garcia, J. Reaction-path dynamics calculations of the $Cl + NH_3$ hydrogen abstraction reaction: The role of the intermediate complex. *J. Phys. Chem. A* **2010**, *114*, 4418−4426.
(41) Li, J.; Li, Y.; Guo, H. Communication. Covalent nature of the $X\cdots H_2O$ (X = F, Cl, Br) interactions. *J. Chem. Phys.* **2013**, *138*, 141102.
(42) Roueff, E.; Lique, F. Molecular excitation in the interstellar medium: Recent advances in collisional, radiative, and chemical processes. *Chem. Rev.* **2013**, *113*, 8906−8938.
(43) Shuman, N. S.; Hunton, D. E.; Viggiano, A. A. Ambient and modified atmospheric ion chemistry: From top to bottom. *Chem. Rev.* **2015**, *115*, 4542−4570.
(44) Chu, T.-S.; Zhang, Y.; Han, K.-L. The time-dependent quantum wave packet approach to the electronically nonadiabatic processes in chemical reactions. *Int. Rev. Phys. Chem.* **2006**, *25*, 201−235.
(45) Guo, H.; Yarkony, D. R. Accurate nonadiabatic dynamics. *Phys. Chem. Chem. Phys.* **2016**, *18*, 26335−26352.
(46) Dawes, R.; Ndengué, S. A. Single- and multireference electronic structure calculations for constructing potential energy surfaces. *Int. Rev. Phys. Chem.* **2016**, *35*, 441−478.
(47) Behler, J. Perspective: Machine learning potentials for atomistic simulations. *J. Chem. Phys.* **2016**, *145*, 170901.
(48) Braams, B. J.; Bowman, J. M. Permutationally invariant potential energy surfaces in high dimensionality. *Int. Rev. Phys. Chem.* **2009**, *28*, 577−606.
(49) Raff, L. M.; Komanduri, R.; Hagan, M.; Bukkapatnam, S. T. S. *Neural Networks in Chemical Reaction Dynamics*; Oxford University Press, 2012.
(50) Manzhos, S.; Dawes, R.; Carrington Jr, T. Neural network-based approaches for building high dimensional and quantum dynamics-friendly potential energy surfaces. *Int. J. Quantum Chem.* **2015**, *115*, 1012−1020.
(51) Jiang, B.; Li, J.; Guo, H. Potential energy surfaces from high fidelity fitting of ab initio points: The permutation invariant polynomial-neural network approach. *Int. Rev. Phys. Chem.* **2016**, *35*, 479−506.
(52) Fu, B.; Zhang, D. H. Ab initio potential energy surfaces and quantum dynamics for polyatomic bimolecular reactions. *J. Chem. Theory Comput.h* **2018**, *14*, 2289−2303.
(53) Dawes, R.; Quintas-Sánchez, E. The construction of ab initio based potential energy surfaces. *Rev. Comput. Chem.* **2018**, *31*, 199−263.
(54) Qu, C.; Yu, Q.; Bowman, J. M. Permutationally invariant potential energy surfaces. *Annu. Rev. Phys. Chem.* **2018**, *69*, 151−175.
(55) Jiang, B.; Li, J.; Guo, H. High-fidelity potential energy surfaces for gas phase and gas-surface scattering processes from machine learning. *J. Phys. Chem. Lett.* **2020**, *11*, 5120−5131.
(56) Czakó, G.; Győri, T.; Papp, D.; Tajti, V.; Tasi, D. A. First-principles reaction dynamics beyond six-atom systems. *J. Phys. Chem. A* **2021**, *125*, 2385−2393.
(57) Zhang, J. Z. H. *Theory and Application of Quantum Molecular Dynamics*; World Scientific, 1999.
(58) Kosloff, R. Propagation methods for quantum molecular dynamics. *Annu. Rev. Phys. Chem.* **1994**, *45*, 145.
(59) Guo, H. Chebyshev propagation and applications to scattering problems. In *Theory of Chemical Reaction Dynamics*; Lagana, A., Lendvay, G., Eds.; Kluwer, 2004; pp 217−229.
(60) Judson, R. S.; Kouri, D. J.; Neuhauser, D.; Baer, M. Time-dependent wave-packet method for the complete determination of S-matrix elements for reactive molecular collisions in three dimensions. *Phys. Rev. A* **1990**, *42*, 351.
(61) Zhang, D. H.; Zhang, J. Z. H. Full-dimensional time-dependent treatment for diatom-diatom reactions: The H_2+OH reaction. *J. Chem. Phys.* **1994**, *101*, 1146−1156.
(62) Yang, M. Full dimensional time-dependent quantum dynamics study of the $H+NH_3 \rightarrow H_2+NH_2$ reaction. *J. Chem. Phys.* **2008**, *129*, 064315.
(63) Wang, D. A full dimensional, nine-degree-of-freedom, time-dependent quantum dynamics study for the H_2+C_2H reaction. *J. Chem. Phys.* **2006**, *124*, 201105.
(64) Hu, Q.; Song, H.; Johnson, C. J.; Li, J.; Guo, H.; Continetti, R. E. Imaging a multidimensional multichannel potential energy surface: Photodetachment of $H^-(NH_3)$ and NH_4^-. *J. Chem. Phys.* **2016**, *144*, 244311.
(65) Song, H.; Yang, M.; Guo, H. Communication: Equivalence between symmetric and antisymmetric stretching modes of NH_3 in promoting $H + NH_3 \rightarrow H_2 + NH_2$ reaction. *J. Chem. Phys.* **2016**, *145*, 131101.

https://doi.org/10.1021/acsphyschemau.3c00009
ACS Phys. Chem Au 2023, 3, 406−418

(66) Tian, L.; Song, H.; Yang, M. Effects of bending excitation on the reaction dynamics of fluorine atoms with ammonia. *Phys. Chem. Chem. Phys.* **2021**, *23*, 2715−2722.
(67) Zare, R. N. *Angular Momentum*; Wiley, 1988.
(68) Fleck, J. A., Jr.; Morris, J. R.; Feit, M. D. Time-dependent propagation of high energy laser beam through the atmosphere. *Appl. Phys.* **1976**, *10*, 129−160.
(69) Mandelshtam, V. A.; Taylor, H. S. A simple recursion polynomial expansion of the Green's function with absorbing boundary conditions. Application to the reactive scattering. *J. Chem. Phys.* **1995**, *103*, 2903−2907.
(70) Chen, R.; Guo, H. Evolution of quantum system in order domain of Chebychev operator. *J. Chem. Phys.* **1996**, *105*, 3569−3578.
(71) Gray, S. K.; Balint-Kurti, G. G. Quantum dynamics with real wavepackets, including application to three-dimensional (J = 0) D+H_2 → HD+H reactive scattering. *J. Chem. Phys.* **1998**, *108*, 950−962.
(72) Chen, R.; Guo, H. Discrete energy representation and generalized propagation of physical systems. *J. Chem. Phys.* **1998**, *108*, 6068.
(73) Tal-Ezer, H.; Kosloff, R. An accurate and efficient scheme for propagating the time dependent Schroedinger equation. *J. Chem. Phys.* **1984**, *81*, 3967−3971.
(74) Sun, Z.; Lee, S.-Y.; Guo, H.; Zhang, D. H. Comparison of second-order split operator and Chebyshev propagator in wave packet based state-to-state reactive scattering calculations. *J. Chem. Phys.* **2009**, *130*, 174102.
(75) Miller, W. H.; Schwartz, S. D.; Tromp, J. W. Quantum mechanical rate constants for bimolecular reactions. *J. Chem. Phys.* **1983**, *79*, 4889−4899.
(76) Zhao, B.; Guo, H. State-to-state quantum reactive scattering in four-atom systems. *WIRES: Comput. Mol. Sci.* **2017**, *7*, No. e1301.
(77) Truhlar, D. G.; Muckerman, J. T. Reactive scattering cross sections III: Quasiclassical and semiclassical methods. In *Atom-Molecule Collision Theory*; Bernstein, R. B., Ed.; Plenum, 1979; pp 505−566.
(78) Hase, W. L. Classical trajectory simulations: Initial conditions. In *Encyclopedia of Computational Chemistry*; Alinger, N. L., Ed.; Wiley, 1998; Vol. *1*, pp 399−402.
(79) Hase, W. L.; Song, K.; Gordon, M. S. Direct dynamics simulations. *Comput. Sci. Eng.* **2003**, *5*, 36−44.
(80) Schatz, G. C. Quasiclassical trajectory studies of state-resolved bimolecular reactions: Vibrational distributions in triatomic products. *J. Phys. Chem.* **1995**, *99*, 516−524.
(81) Aoiz, F. J.; Bañares, L.; Herrero, V. J. The H + H_2 reactive system. Progress in the study of the simplest reaction. *Int. Rev. Phys. Chem.* **2005**, *24*, 119−190.
(82) Czakó, G.; Bowman, J. M. Reaction dynamics of methane with F, O, Cl, and Br on ab initio potential energy surfaces. *J. Phys. Chem. A* **2014**, *118*, 2839−2864.
(83) Li, J.; Jiang, B.; Song, H.; Ma, J.; Zhao, B.; Dawes, R.; Guo, H. From ab initio potential energy surfaces to state-resolved reactivities: The X + H_2O ↔ HX + OH (X = F, Cl, and O(^{3}P)) reactions. *J. Phys. Chem. A* **2015**, *119*, 4667−4687.
(84) Li, J.; Zhao, B.; Xie, D.; Guo, H. Advances and new challenges to bimolecular reaction dynamics theory. *J. Phys. Chem. Lett.* **2020**, *11*, 8844−8860.
(85) Bonnet, L.; Rayez, J.-C. Quasiclassical trajectory method for molecular scattering processes: necessity of a weighted binning approach. *Chem. Phys. Lett.* **1997**, *277*, 183−190.
(86) Bañares, L.; Aoiz, F. J.; Honvault, P.; Bussery-Honvault, B.; Launay, J. M. Quantum mechanical and quasi-classical trajectory study of the C(^{1}D)+H_2 reaction dynamics. *J. Chem. Phys.* **2003**, *118*, 565−568.
(87) Bonnet, L. Classical dynamics of chemical reactions in a quantum spirit. *Int. Rev. Phys. Chem.* **2013**, *32*, 171−228.
(88) Czakó, G.; Bowman, J. M. Quasiclassical trajectory calculations of correlated product distributions for the F+CHD_3(v_1 = 0,1) reactions using an ab initio potential energy surface. *J. Chem. Phys.* **2009**, *131*, 244302.
(89) Bonnet, L.; Espinosa-Garcia, J. The method of Gaussian weighted trajectories. V. On the 1GB procedure for polyatomic processes. *J. Chem. Phys.* **2010**, *133*, 164108.
(90) Conte, R.; Fu, B.; Kamarchik, E.; Bowman, J. M. A novel Gaussian binning (1GB) analysis of vibrational state distributions in highly excited H_2O from reactive quenching of OH* by H_2. *J. Chem. Phys.* **2013**, *139*, 044104.
(91) Espinosa-García, J.; Monge-Palacios, M. Theoretical study of the F + NH_3 and F + ND_3 reactions: Mechanism and comparison with experiment. *J. Phys. Chem. A* **2011**, *115*, 13759−13763.
(92) Xiao, C.; Shen, G.; Wang, X.; Fan, H.; Yang, X. Crossed beams study on the dynamics of the F-atom reaction with ammonia. *J. Phys. Chem. A* **2010**, *114*, 4520−4523.
(93) Babin, M. C.; DeWitt, M.; Lau, J. A.; Weichman, M. L.; Kim, J. B.; Song, H.; Guo, H.; Neumark, D. M. Observation of resonances in the transition state region of the F + NH_3 reaction using anion photoelectron spectroscopy. *Nat. Chem.* **2023**, *15*, 194−199.
(94) Stone, D.; Whalley, L. K.; Heard, D. E. Tropospheric OH and HO_2 radicals: field measurements and model comparisons. *Chem. Soc. Rev.* **2012**, *41*, 6348−6404.
(95) Liu, Y.; Bai, M.; Song, H.; Xie, D.; Li, J. Anomalous kinetics of the reaction between OH and HO_2 on an accurate triplet state potential energy surface. *Phys. Chem. Chem. Phys.* **2019**, *21*, 12667−12675.
(96) Liu, Y.; Song, H.; Xie, D.; Li, J.; Guo, H. Mode specificity in the OH + HO_2 → H_2O + O_2 reaction: Enhancement of reactivity by exciting a spectator mode. *J. Am. Chem. Soc.* **2020**, *142*, 3331−3335.
(97) Francisco, J. S.; Muckerman, J. T.; Yu, H.-G. HOCO radical chemistry. *Acc. Chem. Res.* **2010**, *43*, 1519−1526.
(98) Li, J.; Chen, J.; Zhang, D. H.; Guo, H. Quantum and quasi-classical dynamics of the OH + CO → H + CO_2 reaction on a new permutationally invariant neural network potential energy surface. *J. Chem. Phys.* **2014**, *140*, 044327.
(99) Liu, S.; Chen, J.; Fu, B.; Zhang, D. H. State-to-state quantum versus classical dynamics study of the OH + CO → H + CO_2 reaction in full dimensions (J = 0): checking the validity of the quasi-classical trajectory method. *Theor. Chem. Acc.* **2014**, *133*, 1558.
(100) Caracciolo, A.; Lu, D.; Balucani, N.; Vanuzzo, G.; Stranges, D.; Wang, X.; Li, J.; Guo, H.; Casavecchia, P. Combined experimental-theoretical study of the OH + CO → H + CO_2 reaction dynamics. *J. Phys. Chem. Lett.* **2018**, *9*, 1229−1236.
(101) Li, J.; Wang, Y.; Jiang, B.; Ma, J.; Dawes, R.; Xie, D.; Bowman, J. M.; Guo, H. Communication: A chemically accurate global potential energy surface for the HO + CO → H + CO_2 reaction. *J. Chem. Phys.* **2012**, *136*, 041103.
(102) Chen, J.; Xu, X.; Xu, X.; Zhang, D. H. Communication: An accurate global potential energy surface for the OH + CO → H + CO_2 reaction using neural networks. *J. Chem. Phys.* **2013**, *138*, 221104.
(103) Pan, M.; Xiang, H.; Li, Y.; Song, H. Study on the kinetics and dynamics of the H_2 + NH_2^- reaction on a high-level ab initio potential energy surface. *Phys. Chem. Chem. Phys.* **2021**, *23*, 17848−17855.
(104) Song, K.; Song, H.; Li, J. Validating experiments for the reaction H_2 + NH_2^- by dynamical calculations on an accurate full-dimensional potential energy surface. *Phys. Chem. Chem. Phys.* **2022**, *24*, 10160−10167.
(105) Song, H.; Li, A.; Guo, H. Rotational and isotopic effects in the H_2 + OH^+ → H + H_2O^+ reaction. *J. Phys. Chem. A* **2016**, *120*, 4742−4748.
(106) Lu, D.; Li, J.; Guo, H. Stereodynamical control of product branching in multi-channel barrierless hydrogen abstraction of CH_3OH by F. *Chem. Sci.* **2019**, *10*, 7994−8001.
(107) Toscano, J.; Lewandowski, H. J.; Heazlewood, B. R. Cold and controlled chemical reaction dynamics. *Phys. Chem. Chem. Phys.* **2020**, *22*, 9180−9194.
(108) Sabbah, H.; Biennier, L.; Sims, I. R.; Georgievskii, Y.; Klippenstein, S. J.; Smith, I. W. M. Understanding reactivity at very low temperatures: The reactions of oxygen atoms with alkenes. *Science* **2007**, *317*, 102−105.

https://doi.org/10.1021/acsphyschemau.3c00009
ACS Phys. Chem Au 2023, 3, 406−418

(109) Herbst, E.; Klemperer, W. Formation and depletion of molecules in dense interstellar clouds. *Astrophys. J.* **1973**, *185*, 505−533.
(110) Li, A.; Guo, H. A nine-dimensional ab initio global potential energy surface for the $H_2O^+ + H_2 \rightarrow H_3O^+ + H$ reaction. *J. Chem. Phys.* **2014**, *140*, 224313.
(111) Ard, S. G.; Li, A.; Martinez, O.; Shuman, N. S.; Viggiano, A. A.; Guo, H. Experimental and theoretical kinetics for the $H_2O^+ + H_2/D_2 \rightarrow H_3O^+/H_2DO^+ + H/D$ reactions: Observation of the rotational Effect in the temperature dependence. *J. Phys. Chem. A* **2014**, *118*, 11485−11489.
(112) Song, H.; Li, A.; Guo, H.; Xu, Y.; Xiong, B.; Chang, Y. C.; Ng, C. Comparison of experimental and theoretical quantum-state-selected integral cross sections for the $H_2O^+ + H_2$ (D_2) reactions in the collision energy range of 0.04−10.00 eV. *Phys. Chem. Chem. Phys.* **2016**, *18*, 22509−22515.
(113) Song, H.; Li, A.; Yang, M.; Guo, H. Competition between the H- and D-atom transfer channels in the $H_2O^+ + HD$ reaction: reduced-dimensional quantum and quasi-classical studies. *Phys. Chem. Chem. Phys.* **2017**, *19*, 17396−17403.
(114) Li, A.; Guo, H. A full-dimensional ab initio global potential energy surface of $H_3O^+(\tilde{a}^3A)$ for the $OH^+(\tilde{X}^3\Sigma^-) + H_2(\tilde{X}^1\Sigma_g^+) \rightarrow H(^2S) + H_2O^+(\tilde{X}^2B_1)$ reaction. *J. Phys. Chem. A* **2014**, *118*, 11168−11176.
(115) Martinez, O.; Ard, S. G.; Li, A.; Shuman, N. S.; Guo, H.; Viggiano, A. A. Temperature-dependent kinetic measurements and quasi-classical trajectory studies for the $OH^+ + H_2/D_2 \rightarrow H_2O+/HDO^+ + H/D$ reactions. *J. Chem. Phys.* **2015**, *143*, 114310.
(116) Espinosa-Garcia, J.; Fernandez-Ramos, A.; Suleimanov, Y. V.; Corchado, J. C. Theoretical study of the $F(^2P) + NH_3$ hydrogen abstraction reaction: Mechanism and kinetics. *J. Phys. Chem. A* **2014**, *118*, 554−560.
(117) Lu, D.-d.; Xie, C.-j.; Li, J.; Guo, H. Rate coefficients and branching ratio for multi-channel hydrogen abstractions from CH_3OH by F. *Chin. J. Chem. Phys.* **2019**, *32*, 84−88.
(118) Lu, D.; Li, J.; Guo, H. Comprehensive dynamical investigations on the $Cl + CH_3OH \rightarrow HCl + CH_3O/CH_2OH$ reaction: Validation of experiment and dynamical insights. *CCS Chem.* **2020**, *2*, 882−894.
(119) Xu, Y.; Xiong, B.; Chang, Y. C.; Ng, C. Y. Communication: Rovibrationally selected absolute total cross sections for the reaction $H_2O^+(X^2B_1; v_1^+v_2^+v_3^+=000; N^+K_a^+K_c^+) + D_2$: Observation of the rotational enhancement effect. *J. Chem. Phys.* **2012**, *137*, 241101.
(120) Xu, Y.; Xiong, B.; Chang, Y. C.; Ng, C. Y. The translational, rotational, and vibrational energy effects on the chemical reactivity of water cation $H_2O^+(X^2B_1)$ in the collision with deuterium molecule D_2. *J. Chem. Phys.* **2013**, *139*, 024203.
(121) Li, A.; Li, Y.; Guo, H.; Lau, K.-C.; Xu, Y.; Xiong, B.; Chang, Y.-C.; Ng, C. Y. Communication: The origin of rotational enhancement effect for the reaction $H_2O^+ + H_2$ (D_2). *J. Chem. Phys.* **2014**, *140*, 011102.
(122) Ping, L.; Zhu, Y.; Li, A.; Song, H.; Li, Y.; Yang, M. Dynamics and kinetics of the reaction $OH + H_2S \rightarrow H_2O + SH$ on an accurate potential energy surface. *Phys. Chem. Chem. Phys.* **2018**, *20*, 26315−26324.
(123) Xiang, H.; Lu, Y.; Song, H.; Yang, M. Mode-specific quantum dynamics study of $OH + H_2S \rightarrow H_2O + SH$ reaction. *Chin. J. Chem. Phys.* **2022**, *35*, 200−206.
(124) Spencer, J. E.; Glass, G. P. Some reactions of OH(v = 1). *Int. J. Chem. Kinet.* **1977**, *9*, 111−122.
(125) Li, J.; Xie, C.; Ma, J.; Wang, Y.; Dawes, R.; Xie, D.; Bowman, J. M.; Guo, H. Quasi-classical dynamics of the $HO + CO \rightarrow H + CO_2$ reaction on a new ab initio based potential energy surface. *J. Phys. Chem. A* **2012**, *116*, 5057−5067.
(126) Zhu, Y.; Li, R.; Song, H. Kinetic and dynamic studies of the $NH_2^+ + H_2$ reaction on a high-level ab initio potential energy surface. *Phys. Chem. Chem. Phys.* **2022**, *24*, 25663−25672.
(127) Troe, J. Recent advances in statistical adiabatic channel calculations of state-specific dissociation dynamics. *Adv. Chem. Phys.* **2007**, *101*, 817−852.
(128) González-Lezana, T. Statistical quantum studies on insertion atom-diatom reactions. *Int. Rev. Phys. Chem.* **2007**, *26*, 29−91.
(129) Sun, Z.; Zhang, D. H.; Xu, C.; Zhou, S.; Xie, D.; Lendvay, G.; Lee, S.-Y.; Lin, S. Y.; Guo, H. State-to-state dynamics of $H + O_2$ reaction. Evidence for nonstatistical behavior. *J. Am. Chem. Soc.* **2008**, *130*, 14962−14963.
(130) Sun, Z.; Liu, L.; Lin, S. Y.; Schinke, R.; Guo, H.; Zhang, D. H. State-to-state quantum dynamics of $O + O_2$ isotope exchange reactions reveals non-statistical behavior at atmospheric conditions. *Proc. Natl. Acad. Sci. U.S.A.* **2010**, *107*, 555−558.
(131) Chen, G. K.; Xie, C.; Yang, T.; Li, A.; Suits, A. G.; Hudson, E. R.; Campbell, W. C.; Guo, H. Isotope-selective chemistry in the $Be^+(^2S_{1/2}) + HOD \rightarrow BeOD^+/BeOH^+ + H/D$ reaction. *Phys. Chem. Chem. Phys.* **2019**, *21*, 14005−14011.
(132) Xie, C.; Liu, X.; Sweeny, B. C.; Miller, T. M.; Ard, S. G.; Shuman, N. S.; Viggiano, A. A.; Guo, H. Probing the rate-determining region of the potential energy surface for a prototypical ion−molecule reaction. *Philos. Trans. Royal Soc. A* **2018**, *376*, 20170146.
(133) Sloan, J. J.; Watson, D. G.; Williamson, J. The detailed isotope effect in the $F + NH_3$ and $F + ND_3$ reactions. *Chem. Phys. Lett.* **1980**, *74*, 481−485.
(134) Wategaonkar, S.; Setser, D. W. Vibrational energy disposal in the reactions of F atoms with NH_3, ND_3, N_2H_4, and CH_3ND_2. *J. Chem. Phys.* **1987**, *86*, 4477−4487.
(135) Szabó, I.; Czakó, G. Dynamics and novel mechanisms of S_N2 reactions on ab initio analytical potential energy surfaces. *J. Phys. Chem. A* **2017**, *121*, 9005−9019.
(136) Lehman, J. H.; Lester, M. I. Dynamical outcomes of quenching: Reflections on a conical intersection. *Annu. Rev. Phys. Chem.* **2014**, *65*, 537−555.
(137) Westermann, T.; Kim, J. B.; Weichman, M. L.; Hock, C.; Yacovitch, T. I.; Palma, J.; Neumark, D. M.; Manthe, U. Resonances in the entrance channel of the elementary chemical reaction of fluorine and methane. *Angew. Chem., Int. Ed.* **2014**, *53*, 1122−1126.
(138) Zhao, B.; Manthe, U. Non-adiabatic transitions in the reaction of fluorine with methane. *J. Chem. Phys.* **2020**, *152*, 231102.
(139) Zhao, B.; Han, S.; Malbon, C. L.; Manthe, U.; Yarkony, D. R.; Guo, H. Full-dimensional quantum stereodynamics of the non-adiabatic quenching of $OH(A^2\Sigma^+)$ by H_2. *Nat. Chem.* **2021**, *13*, 909−915.
(140) Jasper, A. W.; Nangia, S.; Zhu, C.; Truhlar, D. G. Non-Born-Oppenheimer molecular dynamics. *Acc. Chem. Res.* **2006**, *39*, 101−108.
(141) Willitsch, S. Coulomb-crystallised molecular ions in traps: methods, applications, prospects. *Int. Rev. Phys. Chem.* **2012**, *31*, 175−199.
(142) van de Meerakker, S. Y. T.; Bethlem, H. L.; Vanhaecke, N.; Meijer, G. Manipulation and control of molecular beams. *Chem. Rev.* **2012**, *112*, 4828−4878.
(143) Narevicius, E.; Raizen, M. G. Toward cold chemistry with magnetically decelerated supersonic beams. *Chem. Rev.* **2012**, *112*, 4879−4889.
(144) Jankunas, J.; Osterwalder, A. Cold and controlled molecular beams: Production and applications. *Annu. Rev. Phys. Chem.* **2015**, *66*, 241−262.
(145) Bohn, J. L.; Rey, A. M.; Ye, J. Cold molecules: Progress in quantum engineering of chemistry and quantum matter. *Science* **2017**, *357*, 1002−1010.
(146) Fournier, M.; Le Picard, S. D.; Sims, I. R. Low-temperature Chemistry in Uniform Supersonic Flows. In *Cold Chemistry: Molecular Scattering and Reactivity Near Absolute Zero*; Dulieu, O., Osterwalder, A., Eds.; RSC Publishing, 2018; pp 1−45.
(147) Mukherjee, N. Quantum-controlled collisions of H_2 molecules. *J. Phys. Chem. A* **2023**, *127*, 418−438.
(148) Krems, R. V. Cold controlled chemistry. *Phys. Chem. Chem. Phys.* **2008**, *10*, 4079−4092.
(149) Balakrishnan, N. Perspective: Ultracold molecules and the dawn of cold controlled chemistry. *J. Chem. Phys.* **2016**, *145*, 150901.
(150) Hu, M.-G.; Liu, Y.; Nichols, M. A.; Zhu, L.; Quéméner, G.; Dulieu, O.; Ni, K.-K. Nuclear spin conservation enables state-to-state

control of ultracold molecular reactions. *Nat. Chem.* **2021**, *13*, 435−440.
(151) Liu, Y.; Hu, M.-G.; Nichols, M. A.; Yang, D.; Xie, D.; Guo, H.; Ni, K.-K. Precision test of statistical dynamics with state-to-state ultracold chemistry. *Nature* **2021**, *593*, 379−384.
(152) Liu, Y.; Hu, M.-G.; Nichols, M. A.; Grimes, D. D.; Karman, T.; Guo, H.; Ni, K.-K. Photo-excitation of long-lived transient intermediates in ultracold reactions. *Nat. Phys.* **2020**, *16*, 1132−1136.
(153) Yang, D.; Huang, J.; Hu, X.; Xie, D.; Guo, H. Statistical quantum mechanical approach to diatom-diatom capture dynamics and application to ultracold KRb + KRb reaction. *J. Chem. Phys.* **2020**, *152*, 241103.
(154) Ma, J.; Li, J.; Guo, H. Quantum dynamics of the HO + CO → H + CO_2 reaction on an accurate potential energy surface. *J. Phys. Chem. Lett.* **2012**, *3*, 2482−2486.

https://doi.org/10.1021/acsphyschemau.3c00009
ACS Phys. Chem Au 2023, 3, 406−418